Neutrophil microparticle production and inflammasome activation by hyperglycemia due to cytoskeletal instability

Received for publication, June 16, 2017, and in revised form, September 11, 2017 Published, Papers in Press, September 25, 2017, DOI 10.1074/jbc.M117.802629

Stephen R. Thom[‡1], **Veena M. Bhopale**[‡], **Kevin Yu**[‡], **Weiliang Huang**[§], **Maureen A. Kane**[§], **and David J. Margolis**[¶]

From the [‡]*Department of Emergency Medicine, School of Medicine, and* [§]*Department of Pharmaceutical Sciences, School of Pharmacy, University of Maryland, Baltimore, Maryland 21201 and the* [¶]*Department of Dermatology and Department of Biostatistics and Epidemiology, Perelman School of Medicine, University of Pennsylvania, Philadelphia, Pennsylvania 19104*

Edited by Luke O'Neill

Microparticles are lipid bilayer–enclosed vesicles produced by cells under oxidative stress. MP production is elevated in patients with diabetes, but the underlying cellular mechanisms are poorly understood. We hypothesized that raising glucose above the physiological level of 5.5 mM would stimulate leukocytes to produce MPs and activate the nucleotide-binding domain, leucine-rich repeat pyrin domain–containing 3 (NLRP3) inflammasome. We found that when incubated in buffer with up to 20 mM glucose, human and murine neutrophils, but not monocytes, generate progressively more MPs with high interleukin (IL)-1β content. Enhanced MP production required generation of reactive chemical species by mitochondria, NADPH oxidase, and type 2 nitric-oxide synthase (NOS-2) and resulted in *S*-nitrosylation of actin. Depleting cells of capon (C-terminal PDZ ligand of neuronal nitric-oxide synthase protein), apoptosis-associated speck-like protein containing C-terminal caspase recruitment domain (ASC), or pro-IL-1β prevented the hyperglycemia-induced enhancement of reactive species production, MP generation, and IL-1β synthesis. Additional components required for these responses included inositol 1,3,5-triphosphate receptors, PKC, and enhancement of filamentous-actin turnover. Numerous proteins become localized to short filamentous actin in response to *S*-nitrosylation, including vasodilator-stimulated phosphoprotein, focal adhesion kinase, the membrane phospholipid translocation enzymes flippase and floppase, capon, NLRP3, and ASC. We conclude that an interdependent oxidative stress response to hyperglycemia perturbs neutrophil cytoskeletal stability leading to MP production and IL-1β synthesis.

Microparticles (MPs)[2] are 0.1- to 1-μm diameter vesicles produced via an outward budding of the cell membrane in response to several stimuli (1). Healthy individuals have blood-borne MPs, and some MPs are 2–10-fold higher in those with types 1 and 2 diabetes mellitus (2–7). Reasons why this elevation occurs, and more generally the cellular mechanisms involved with MP production, are poorly understood. In this study, we investigated MP generation by leukocytes in response to elevations of glucose concentration pertinent to diabetes (6). Leukocyte-derived MPs have adverse effects on healing and play a role in endothelial injury and progression of atherosclerosis (6, 8–11).

Hyperglycemia triggers cells to increase production of mitochondrial reactive oxygen species (ROS) (12). We recently reported a mechanism whereby mitochondrial ROS play a role in MP production in response to elevations of carbon dioxide, and we hypothesized that similar events may occur due to hyperglycemia (13). We reported that MP production by human and murine neutrophils involves ROS production from both mitochondria and NADPH oxidase (Nox) and also requires activity of type 2 or inflammatory nitric-oxide synthase (NOS-2). These events lead to *S*-nitrosylation of cytosolic actin, increased actin reorganization/turnover, and activation of phospholipid transporters (13, 14). The complexity and similarity of the response pattern for different stimuli suggested to us that it may represent a virtual leitmotif for MP production. Activation of Nox is central to MP generation in response to several stimuli (13–15), and there are several pathways by which mitochondrial reactive species can activate Nox (12, 16).

Interleukin (IL)-1β production via the NLRP3 inflammasome is intimately associated with both oxidant production and MP production formation (13, 17). Therefore, we investigated whether IL-1β production also occurred as part of the MP generation scheme. IL-1β is synthesized without a leader peptide so it cannot utilize the conventional secretory pathway (endoplasmic reticulum–Golgi–plasma membrane). IL-1β packaging into MPs for secretion has been described (13, 18–20). Moreover, several studies have demonstrated that diabetic nephropathy, retinopathy, and endothelial dysfunction

This work was supported by National Institutes of Health Grant R01-DK094260 from NIDDK (to S. R. T. and D. J. M.), Office of Naval Research Grant N00014-16-1-2868 (to S. R. T.), and University of Maryland Baltimore, School of Pharmacy Mass Spectrometry Center Grant SOP1841-IQB2014 (to W. H. and M. A. K.). The authors declare that they have no conflicts of interest with the contents of this article. The content is solely the responsibility of the authors and does not necessarily represent the official views of the National Institutes of Health.

This article contains supplemental Tables S1–S2.

[1] To whom correspondence should be addressed: Dept. of Emergency Medicine, University of Maryland School of Medicine, 655 W. Baltimore St., Bressler Research Bldg., Rm. 4-013, Baltimore, MD 21201. Tel.: 410-706-8294; Fax: 410-328-8028; E-mail: sthom@em.umaryland.edu.

[2] The abbreviations used are: MP, microparticle; FBE, actin-free barbed ends; ASC, apoptosis-associated speck-like protein containing C-terminal caspase recruitment domain; DCF, 2′,7′-dichlorofluorescein; DCF-DA, 2,7-dihydrodichlorofluorescein diacetate; FAK, focal adhesion kinase; IL-1β, interleukin-1β; IP_3, inositol 1,3,5-triphosphate; Nox, NADPH oxidase; PDI, protein-disulfide isomerase; ROS, reactive oxygen species; SNO-actin, *S*-nitrosylated actin; TrxR, thioredoxin reductase; VASP, vasodilator-stimulated phosphoprotein; FBE, free barbed end; DTSP, dithiobis(succinimidyl propionate); UCP, uncoupling protein; SNP, single nucleotide polymorphism; cmk, chloromethyl ketone.

are linked to the NLRP3 inflammasome (21–23). IL-1β autostimulation also establishes a feed-forward process that amplifies inflammation and worsens type 2 diabetes by contributing to insulin secretory dysfunction and pancreatic β-cell apoptosis (24).

As part of this project, we also investigated whether a protein known as the C-terminal PDZ ligand of neuronal nitric-oxide synthase (capon), or nitric-oxide synthase-1 adaptor protein, is involved with leukocyte responses. This was done because variants of the gene coding for capon have been associated with lower extremity amputations and peripheral neuropathy in those with diabetes, but not among those who do not have diabetes (25). More recently, several single nucleotide polymorphisms (SNPs) were associated with impaired healing and amputations among diabetics (26). Others have found associations between some capon gene variants and the incidence of diabetes among users of various medications, as well as variations in therapeutic efficacy of some hyperglycemic medications (27–30). Capon gene variants may play an inconsistent role in diabetes onset in the general population (31, 32) and increase susceptibility to some infections (33).

Knowledge of how capon influences cell functions is limited. When first identified, capon was shown to interact with neuronal (type 1) NOS and to help regulate nitric oxide production at post-synaptic sites in neurons of the CNS (34–37). However, capon is present in many different cells/organs, and its subcellular localization differs due to alterations in its N- and C-terminal regions and to the bridging proteins with which capon interacts (38, 39). Whereas capon does not directly link with NOS-2 or (endothelial) NOS-3 isoforms, indirect associations are suggested in studies of skeletal muscle regeneration (36, 40). We hypothesized that capon may influence NOS-2 activity and thus impact MP production. We approached this study by comparing responses to hyperglycemia using cells either replete with capon or depleted by previous incubation with small inhibitory RNA (siRNA). To aid with following the results, Fig. 1 depicts a schematic mechanism for MP and IL-1β production based on the data generated in this project.

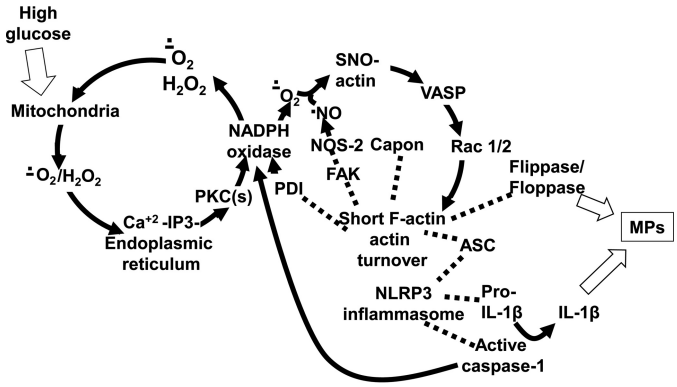

Figure 1. Biochemical mechanism for high glucose–mediated MP production. Data suggest that the initial event triggering MP generation by elevated glucose is enhanced mitochondrial production of reactive species such as superoxide ($O_2^{\cdot-}$) and H_2O_2. These act on endoplasmic reticulum IP_3 receptors, followed by activation of protein kinase C isoforms that increase Nox activity. The data demonstrate an interactive role for agents generated by several enzymes. Therefore, we indicate that Nox-derived $O_2^{\cdot-}$ feeds back to cause further mitochondrial oxidant production and also reacts with nitric oxide ($^{\cdot}NO$) and reactive agents produced by interactions involving these two radical species leading to formation of cytosolic SNO-actin. Actin turnover is enhanced by linkage of VASP to SNO-actin, and accelerated polymerization hastens linkage of Rac 1/2 and FAK that are depicted in the figure with *dotted lines*. FAK links NOS-2 with actin, enhancing its activity. There is also linkage of floppase and flippase to cytosolic actin, which may impact enzyme activity and are required for the membrane phospholipid changes ultimately required for formation. Apoptosis-associated Speck protein with CARD domain (*ASC*) also links to short-filamentous (F)-actin, and the assembled NLRP3 inflammasome, including pro-IL-1β, mediates caspase activation to produce active IL-1β. Activated caspase also feeds back to increase Nox activity. High glucose also triggers an increase in capon linkage to short F-actin, and this relationship is required for NOS-2 activation, which in turn is required for perpetuation of enhanced actin turnover via SNO-actin production.

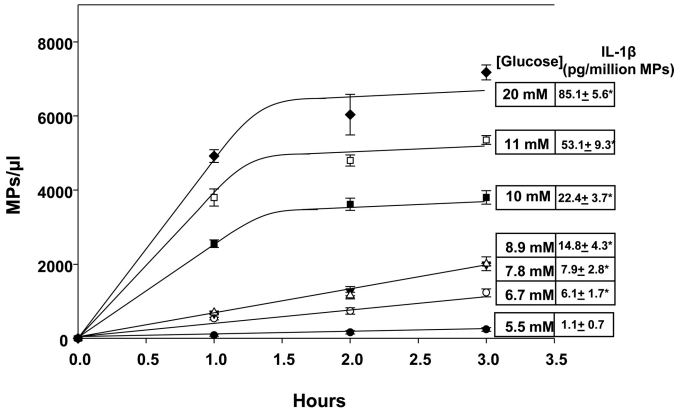

Figure 2. MP production by human neutrophils. MP were counted in suspensions of neutrophils (5.5×10^5/ml in PBS containing 1 mM $CaCl_2$, 1.5 mM $MgCl_2$, and 5.5 to 20 mM glucose) and incubated for the indicated times. MPs were also isolated from suspensions after 2-h incubations, and content of IL-1β was measured. These values are shown in *boxes* to the *right* in the figure. All data shown are mean ± S.E., $n = 4$, *, $p < 0.05$.

Results

Glucose-induced MPs by leukocytes

Leukocytes were isolated from human and mouse blood; the neutrophils and monocytes were separated and then incubated *ex vivo* in buffer with various glucose concentrations. When compared with a physiological glucose concentration of 5.5 mM, human neutrophils exhibited increases in MP production with progressively higher concentrations of glucose (Fig. 2). Mouse neutrophils exhibited a similar response, although they generated only about one-fifth as many MPs as human cells (Fig. 3). Interestingly, neither human nor murine monocytes generated MPs when incubated with 11 or 20 mM glucose for up to 4 h (data not shown).

MP generation could not be attributed to alterations of neutrophil viability, which did not differ significantly across all glucose concentrations (shown in Fig. 3). Additionally, enhanced MP production was not attributable to increased osmolality. For example, in solutions containing 5.5 mM glucose and 14.5 mM mannitol, a non-metabolizable sugar alcohol, murine neutrophils generated no more MPs than in 5.5 mM glucose after incubation for 2 h (0.06 ± 0.01 MPs/cell, $n = 3$).

Proteins required for MP production by neutrophils

Mechanisms for MP generation were investigated using murine neutrophils because unlike human cells they are sufficiently robust to maintain viability during overnight incubations with siRNA to deplete specific proteins. Our mechanistic hypothesis was shaped by prior work showing roles for reactive

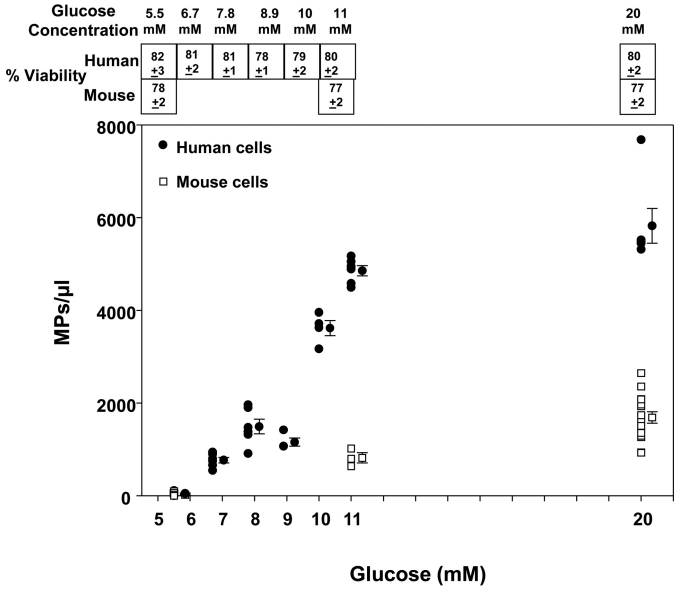

Figure 3. MP production at 2 h by mouse (*open squares*) and human (*closed circles*) neutrophils. Cell suspensions of neutrophils (5.5×10^5/ml in PBS containing 1 mM $CaCl_2$, 1.5 mM $MgCl_2$, and 5.5 to 20 mM glucose) were incubated for 2 h, and individual data points as well as mean ± S.E. bars are shown. Viability of cell preparations at the end of the incubations are shown in *boxes* at the *top* of the figure as mean ± S.E.

species generated by mitochondria, Nox, and NOS-2 to stimulate MP production (13).

As shown in the first two columns of Table 1, we found no significant MP production by cells in 20 mM glucose that were depleted of mitochondrial uncoupling protein 2 (UCP2). The overnight siRNA incubation protocols typically depleted about 80% of the targeted protein, as assessed by Western blottings. Fig. 4 shows results for UCP2 depletion, for example, where siRNA reduced cell content by 85.4 ± 4.3%, $n = 4$. Depletion of the gp91phox subunit of Nox (reduced cell content by 84.4 ± 4.3%, $n = 4$) had a similar effect on MP production by hyperglycemia (Table 1).

A role for NOS-2 was shown by lack of MP generation using cells from NOS-2 knock-out mice. Consistent with these results, no significant increase in MP production was found when wild-type cells were incubated in buffer containing ebselen (an anti-oxidant), genepin (a UCP inhibitor), 1400W (a NOS-2 inhibitor), and Nox2ds (a small peptide inhibitor of Nox) but not to the scrambled sequence control peptide to Nox2ds. Inhibition was also seen with cytochalasin D, indicating a role for actin turnover.

From prior work we hypothesize that a close relationship exists between MP generation and NLRP3 inflammasome activation (13). When cells were depleted of ASC, which serves as a platform for inflammasome oligomerization (41) using siRNA (reduced cell content by 86.6 ± 3.4%, $n = 3$), no enhanced MP production occurred. A similar inhibitory effect occurred when cells were depleted of pro-IL-1β (siRNA reduced cell content by 95.7 ± 1.4%, $n = 3$), which is also incorporated into the inflammasome during activation (42). Once fully formed, the inflammasome activates caspase-1 (in humans, or −11 in mice). We found (Table 1) that incubating cells with a membrane-permeable caspase inhibitor, Ac-YVAD-cmk, also abrogates responses to 20 mM glucose.

MP production was also inhibited when cells were depleted of the type 2 endoplasmic reticulum inositol 1,3,5-triphosphate (IP_3) receptor (cell content was reduced by 91.6 ± 3.5%, $n = 4$), when incubated with 2-aminoethoxydiphenyl borate, an IP_3 inhibitor, and when incubated with GF 109203X, a PKC inhibitor. Finally, no enhanced MP production occurred with cells depleted of capon (siRNA reduced cell content by 73.4 ± 3.4%, $n = 4$).

Glucose-induced elevation of IL-1β content in MPs

The concentration of IL-1β in MPs generated by neutrophils increased when cells were incubated in buffer containing elevated glucose concentrations. The IL-1β concentration in MPs generated by human cells incubated with various glucose concentrations is shown in the *right margin* in Fig. 2. The concentration of IL-1β in mouse MPs also increased with high glucose, and values are listed in the second two columns of Table 1. As shown, inhibition or depletion of proteins required for glucose-induced MP production also abolished elevations in IL-1β concentration.

The NLRP3 inflammasome can also trigger activation of IL-18, which is similar in structure to IL-1β. We found, however, no significant increase in IL-18 occurred in MPs generated by murine neutrophils. IL-18 content of MPs generated by neutrophils incubated in 5.5 mM glucose for 2 h was 12.7 ± 1.5 ($n = 4$) and after incubation in 20 mM glucose 10.5 ± 1.6 ($n = 4$, not significantly different) pg/million MPs.

Reactive species generation by high glucose

Mitochondrial activity in murine neutrophils was probed by assessing fluorescence of MitoSOX Red, which increased linearly at nearly twice the rate when cells were incubated with 20 mM glucose *versus* 5.5 mM glucose (Fig. 5, *A*). Studies were performed with all agents that inhibited glucose-enhanced MPs and IL-1β production, and each also abrogated the increase in MitoSOX Red fluorescence (third set of two columns in Table 1).

To gain further insight into neutrophil-reactive species generation, cells were loaded with the redox active agent 2,7-dihydrodichlorofluorescein diacetate (DCF-DA) and fluorescence-monitored (Fig. 5, *B*). An enhanced rate was found after cells had been exposed to 11 or 20 mM glucose. Moreover, all agents that inhibited glucose-enhanced MPs, IL-1β production, and MitoSOX Red fluorescence also abolished the increase in DCF fluorescence (fourth set of two columns in Table 1).

Actin S-nitrosylation

MPs were not generated by high glucose using neutrophils from NOS-2 KO mice, when gp91phox was depleted, or with cells exposed to the specific inhibitors 1400 W or Nox2ds. Many of the more highly reactive species generated by reactions between nitric oxide and ROS can cause protein *S*-nitrosylation. *S*-Nitrosylation of murine neutrophil proteins was surveyed by the biotin-switch assay, which covalently adds a disulfide-linked biotin to the labile *S*-nitrosylation (SNO-) sites on proteins.

Fig. 6 is a representative Western blot probed for biotin-containing proteins in cells incubated in 5.5 mM *versus* 20 mM

Table 1

Impact of various agents on 5.5 *versus* 20 mM glucose-exposed neutrophil MP production, MP IL-1β concentration, MitoSOX Red, and DCF-DA fluorescence

The isolated murine neutrophils (5.5×10^5/ml PBS containing 1 mM $CaCl_2$, 1.5 mM $MgCl_2$, and 5.5 mM or 20 mM glucose) were incubated for up to 2 h. MPs/PMN reflects increases in MPs in suspensions of 550 neutrophils over 2 h. MitoSOX reflects fluorescence from cells incubated with 5 μM MitoSOX Red for 10 min, washed, and then incubated in buffer for up to 2 h. DCF fluorescence was assessed when 10 μM DCF-DA was added to cell suspensions at the end of 2-h incubations. All values are mean ± S.E. (n = number of independent trials). Abbreviations and manipulations are as follows: KO, neutrophils from NOS-2 knock-out mice; 1400W, incubation with 1 mM 1400W; Nox2ds, incubation with 10 μM Nox2ds, a peptidic inhibitor that mimics a sequence in the cytosolic B loop of Nox2; Scrmb-Nox2ds, incubations performed with 10 μM control, scrambled sequence peptide to Nox2ds; Cont-si cells incubated with control, scrambled sequence siRNA for 20 h prior to the experiment; Capon si, cells incubated with siRNA specific to capon for 20 h prior to the experiment; UCP2si, cells incubated with siRNA specific to uncoupling protein 2 for 20 h prior to the experiment; genepin, incubation with 5 μM genipin, a UCP inhibitor, during a 2-h study; IP3si, cells incubated with siRNA specific to the inositol 1,4,5-trisphosphate receptor type 2 for 20 h prior to the experiment; APB, incubation with 100 μM 2-aminoethoxydiphenyl borate, an IP_3 receptor inhibitor during a 2-h study; GF 109203X, incubation with 5 μM of the protein kinase C inhibitor during a 2-h study; ebselen, incubation with 1 mM of the antioxidant during a 2-h study; UV, cells incubated for 30 min and then to UV light for 5 min and incubated for the remainder of 2 h prior to assays; Cyto D, incubation with 5 μM cytochalasin D during a 2-h study; ASCsi, cells incubated with siRNA specific to ASC for 20 h prior to the experiment; pro-IL-1β siRNA, cells incubated with siRNA specific to pro-IL-1β for 20 h prior to the experiment; Ac-YVAD-cmk, cells incubated with 50 μM Ac-YVAD-cmk, a caspase inhibitor, during a 2-h study.

	MPs/PMN		pg IL-1β/million MPs		MitoSox (fluorescence/min)		DCF (fluorescence/min)	
	5.5 mM	20 mM	5.5 mM	20 mM	5.5 mM	20 mM	5.5 mM	20 mM
PBS	0.05 ± 0.02 (8)	2.9 ± 0.4 (8)[a]	1.6 ± 0.3 (8)	14.1 ± 1.9 (8)	13.2 ± 0.1 (8)	19.9 ± 0.1 (8)[a]	1.2 ± 0.1 (8)	5.6 ± 0.2 (8)[a]
NOS KO	0.08 ± 0.03 (5)	0.04 ± 0.01 (5)	ND	ND	13.3 ± 0.2 (4)	13.1 ± 0.1 (4)	1.5 ± 0.2 (4)	1.6 ± 0.1 (4)
1400W	0.02 ± 0.01 (5)	0.01 ± 0.06 (5)	1.6 ± 0.4 (3)	1.7 ± 0.4 (3)	12.8 ± 0.1 (4)	13.3 ± 0.1 (4)	1.2 ± 0.2 (4)	1.5 ± 0.2 (4)
Nox2ds	0.03 ± 0.02 (5)	0.01 ± 0.09 (5)	1.3 ± 0.3 (3)	1.7 ± 0.8 (3)	13.1 ± 0.1 (4)	13.1 ± 0.1 (4)	1.3 ± 0.3 (4)	1.5 ± 0.3 (4)
Scrmb- Nox2	0.03 ± 0.02 (5)	2.8 ± 0.2 (5)[a]	1.8 ± 0.4 (3)	13.4 ± 1.4 (3)[a]	12.3 ± 0.2 (8)	20.3 ± 0.1 (4)[a]	1.4 ± 0.3 (4)	5.8 ± 0.2 (4)[a]
Control si	0.04 ± 0.03 (8)	3.1 ± 0.2 (8)[a]	1.8 ± 0.2 (8)	13.8 ± 0.4 (8)[a]	12.8 ± 0.1 (8)	19.9 ± 0.1 (8)[a]	1.3 ± 0.2 (8)	5.3 ± 0.4 (8)[a]
$gp9^{Phox}$ si	0.13 ± 0.02 (4)	0.12 ± 0.1 (4)	1.4 ± 0.3 (3)	1.7 ± 0.3 (3)	12.8 ± 0.2 (4)	13.3 ± 0.1 (4)	1.1 ± 0.2 (4)	1.3 ± 0.6 (4)
Capon si	0.03 ± 0.02 (5)	0.11 ± 0.1 (4)	1.4 ± 0.3 (3)	1.7 ± 0.3 (3)	12.9 ± 0.1 (4)	12.9 ± 0.1 (4)	1.3 ± 0.2 (4)	1.5 ± 0.5 (4)
UCP2si	0.12 ± 0.04 (4)	0.11 ± 0.06 (4)	1.4 ± 0.3 (3)	1.7 ± 0.3 (3)	13.3 ± 0.2 (4)	13.4 ± 0.1 (4)	1.2 ± 0.4 (4)	1.9 ± 0.3 (4)
Genepin	0.05 ± 0.06 (5)	0.06 ± 0.06 (5)	1.6 ± 0.4 (3)	1.6 ± 0.5 (3)	12.6 ± 0.1 (4)	13.2 ± 0.1 (4)	1.2 ± 0.3 (4)	1.5 ± 0.3 (4)
IP3si	0.06 ± 0.03 (5)	0.01 ± 0.02 (5)	2.2 ± 0.8 (3)	1.7 ± 0.6 (3)	13.1 ± 0.2 (4)	13.4 ± 0.1 (3)	1.2 ± 0.2 (4)	1.7 ± 0.4 (3)
APB	0.05 ± 0.04 (4)	0.01 ± 0.02 (4)	1.9 ± 0.3 (3)	2.1 ± 0.3 (3)	13.3 ± 0.2 (4)	13.2 ± 0.1 (4)	1.1 ± 0.2 (4)	1.5 ± 0.5 (4)
GF 109203X	0.06 ± 0.03 (5)	0.01 ± 0.02 (5)	2.0 ± 0.6 (3)	2.1 ± 0.7 (3)	13.4 ± 0.1 (4)	13.2 ± 0.1 (4)	1.3 ± 0.2 (4)	1.3 ± 0.4 (4)
UV	0.10 ± 0.04 (8)	0.01 ± 0.03 (8)	1.6 ± 0.5 (3)	1.3 ± 0.4 (3)	12.9 ± 0.3 (4)	13.5 ± 0.1 (4)	1.6 ± 0.2 (4)	1.2 ± 0.2 (4)
Ebselen	0.08 ± 0.02 (3)	0.04 ± 0.01 (3)	1.6 ± 0.4 (4)	2.4 ± 0.9 (4)	12.8 ± 0.1 (3)	12.9 ± 0.3 (3)	1.2 ± 0.1 (3)	1.3 ± 0.4 (3)
Cyto D	0.07 ± 0.03 (5)	0.12 ± 0.09 (5)	1.4 ± 0.4 (3)	1.6 ± 0.9 (3)	12.2 ± 0.2 (4)	13.0 ± 0.4 (4)	1.1 ± 0.1 (4)	1.0 ± 0.3 (4)
ASCsi	0.08 ± 0.03 (4)	0.11 ± 0.08 (4)	1.8 ± 0.2 (3)	1.9 ± 0.5 (3)	12.7 ± 0.2 (4)	13.0 ± 0.2 (4)	1.1 ± 0.1 (4)	1.9 ± 0.3 (4)
Pro-IL-1β siRNA	0.01 ± 0.06 (3)	0.01 ± 0.02 (3)	1.8 ± 0.5 (3)	2.9 ± 0.7 (3)	13.3 ± 0.1 (3)	13.1 ± 0.2 (3)	1.6 ± 0.5 (3)	1.9 ± 0.3 (3)
Ac-YVAD-cmk	0.01 ± 0.02 (3)	0.01 ± 0.01 (3)	1.0 ± 0.7 (3)	2.4 ± 0.9 (3)	13.1 ± 0.1 (3)	13.2 ± 0.1 (3)	1.6 ± 0.1 (3)	2.2 ± 0.4 (3)

[a] $p < 0.05$ *versus* 5.5 mM glucose value.

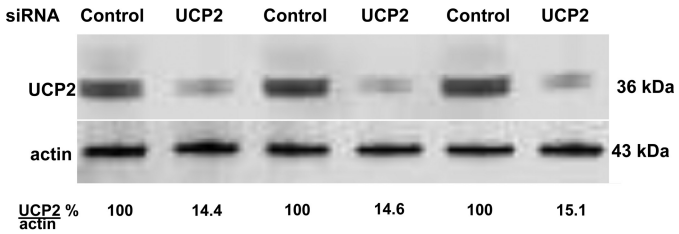

Figure 4. Effect of incubation with siRNA to deplete UCP2 in neutrophils. As an example to demonstrate the efficacy of siRNA to deplete a specific protein in murine neutrophils, Western blot lysates from three different preparations are shown for cells incubated with a control siRNA or siRNA to UCP2. Cytosolic actin from the same lysates are also shown. Ratios shown at the *bottom* were calculated from protein band densities measured in each lysate set.

glucose. Samples labeled with a + were exposed to UV light for 5 min after incubation for 30 min, and then left undisturbed for the remainder of 1 h before the biotin-switch assay was performed. UV light will photo-reverse cysteine *S*-nitrosylation (14). In separate trials, the prominent band at ~43 kDa was cut from nitrocellulose paper, subjected to amino acid sequencing, and identified as actin. Protein loading in each lane of Fig. 6 is shown by the actin band at the bottom. Numbers below the figure reflect the mean (± S.E., $n = 4$) ratio of band densities (biotin/actin). As shown, the ratio was statistically significantly elevated in cells incubated with 20 mM glucose and not exposed to UV light. UV light had no significant effect on cells exposed to 5.5 mM glucose. Moreover, as shown in Table 1, UV light also abrogated hyperglycemia-induced MP generation, MitoSOX, and DCF fluorescence increases, and production of IL-1β in MPs.

Agents generated by reactions between superoxide and nitric oxide can also cause protein nitration. We probed neutrophil lysates for nitrotyrosine and found several faint bands, even with cells incubated at 5.5 mM glucose, and a notably more prominent band at ~70 kDa when cells were incubated with 11 and 20 mM glucose (Fig. 7). Amino acid sequencing identified this protein as a heat-shock cognate 71-kDa protein.

Actin turnover

Actin polymerization was assessed as free barbed end (FBE) formations in murine neutrophils permeabilized so they would take up pyrene-actin. An enhanced rate of actin polymerization occurred when cells were assayed after incubation in 20 mM *versus* 5.5 mM glucose, and this was abrogated by exposure to UV light (Fig. 8) production (43).

Cytoskeletal protein associations based on Triton solubility

We next evaluated associations of cytoplasmic actin with capon and with proteins known to be involved with actin turnover and MP production (13–15, 43–45). After 1-h exposures in buffer equilibrated with 5.5 or 20 mM glucose, neutrophils were incubated with the membrane-permeable protein cross-linker DTSP and then lysed. Cell lysates were separated into Triton-soluble G-actin, short filamentous (sF-) actin, and Triton-insoluble F-actin fractions and subjected to Western blotting. These were analyzed looking for differences in protein-band densities relative to actin. Data shown in Fig. 9 indicate that in the sF-actin fraction of cells incubated in 20 mM glucose, there were marked increases in associations between actin and

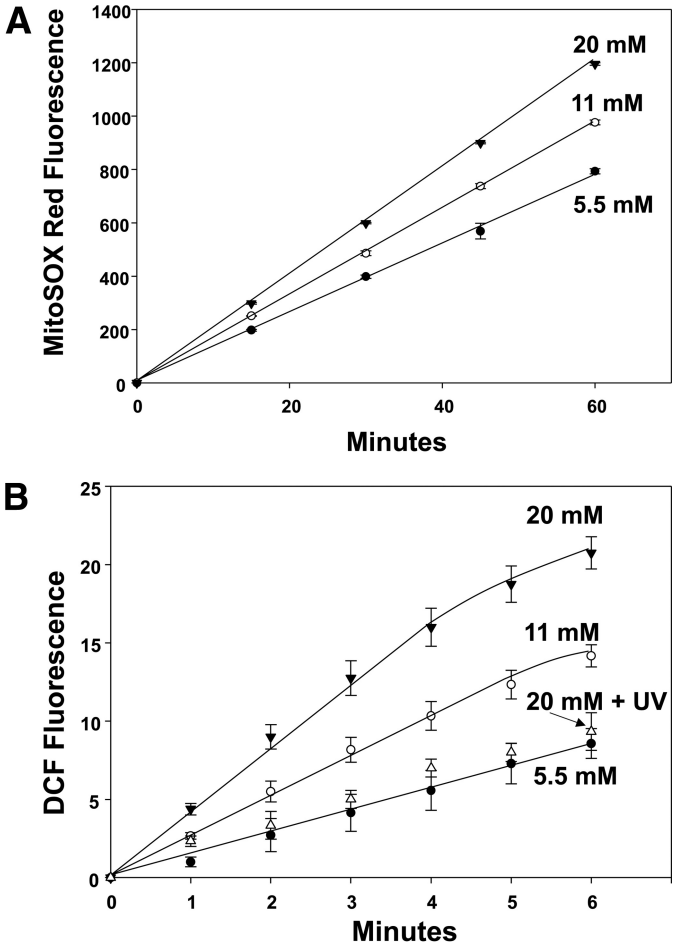

Figure 5. Reactive species production by neutrophils exposed to 5.5, 11, or 20 mM glucose. *A*, murine neutrophils (5.5×10^5/ml PBS containing 1 mM $CaCl_2$, 1.5 mM $MgCl_2$, and 5.5 mM glucose) were first incubated with 5 μM MitoSOX Red for 10 min, and then washed and resuspended in the buffer with different glucose concentrations as shown for up to 1 h. *B*, cells were incubated with the buffer shown for 2 h, and then 10 μM DCF-DA was added, and fluorescence was monitored. Note that when aliquots of cells were incubated in the different glucose concentrations for only 30 min or 1 h, DCF-DA was added, and the same fluorescence rates were measured as for incubations lasting 2 h. This method was chosen because, as discussed under "Experimental procedures," DCF can autocatalyze its own oxidation (79). Values are mean ± S.E., $n = 5$ for each point. Using the same methods, effects of various inhibitors and siRNA depletion of cells are shown in Table 1.

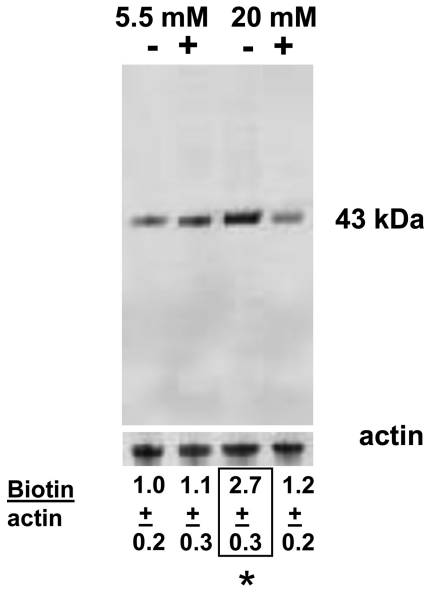

Figure 6. *S*-Nitrosylated protein. Lysates of murine neutrophils incubated in buffer containing 5.5 or 20 mM glucose for 1 h were prepared according to the biotin-switch assay, and the entire blot is shown. + indicates that after 30 min of incubation, cells were exposed to UV light for 5 min and then left for the remainder of 1 h. *Lower blot* shows cytosolic actin in each homogenate to control for protein loading. Ratios reflect results from four replicate studies as mean ± S.E. for individual 43-kDa biotin band density/actin band density of cell lysates normalized to the mean ratio for the 5.5 mM glucose samples.

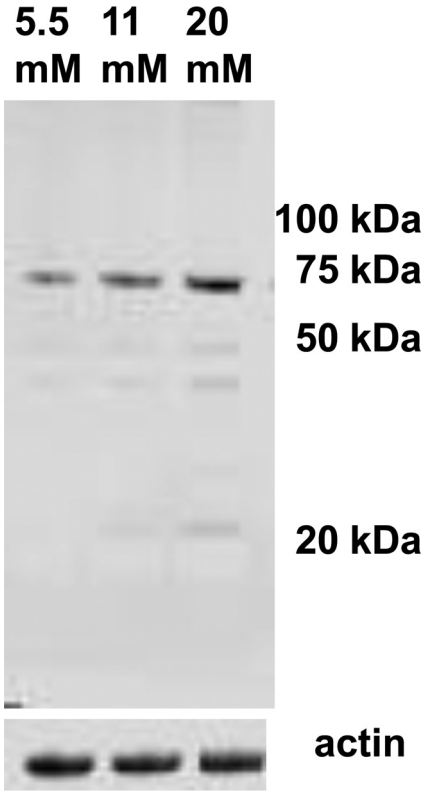

Figure 7. Nitrotyrosine in cell proteins. This is a representative Western blot of lysates from murine neutrophils incubated with 5.5, 11, or 20 mM glucose for 2 h that was probed with an anti-nitrotyrosine antibody.

NOS-2, focal adhesion kinase (FAK), vasodilator-stimulated phosphoprotein (VASP), thioredoxin reductase (TrxR), protein-disulfide isomerase (PDI), flippase, floppase, capon, ASC, and NLRP3. There were reciprocal decreases in these associations with actin in other cytoskeletal fractions, and all the 20 mM glucose-induced changes in protein linkages were abrogated if cells had been exposed to UV light for just 5 min during the 1-h incubation.

Microscopic appearance of capon in neutrophils and effect of capon on glucose-enhanced actin turnover

The intracellular localization and roles for all proteins examined in our study are well known, except for capon. We therefore devoted additional study to the relationship of capon to cytoskeletal actin. The panel of images in Fig. 10 shows that the distribution of F-actin visualized as phalloidin staining was unchanged by incubation in 5.5 *versus* 20 mM glucose, but capon changed from a relatively diffuse cytoplasmic location in 5.5 mM glucose to a dense sub-membranous location following incubation in 20 mM glucose. A similarly more intense sub-

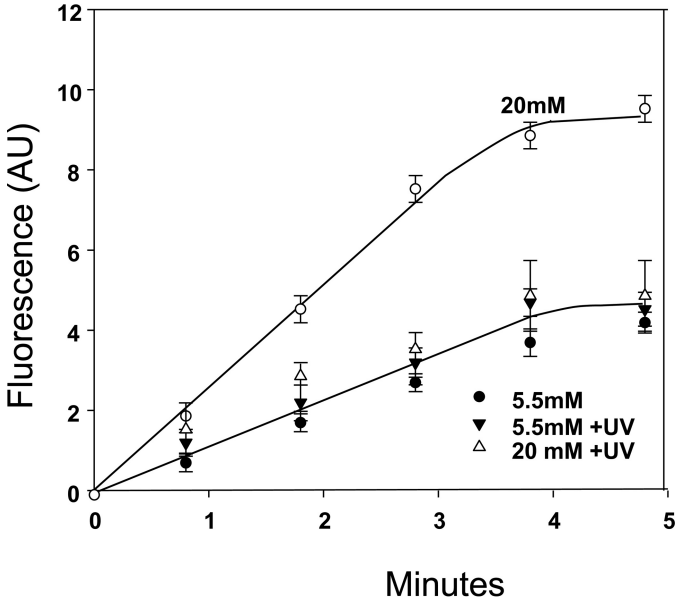

Figure 8. Actin polymerization rate. Permeabilized murine neutrophil suspensions were processed as described under "Experimental procedures" and incubated in buffer containing 5.5 or 20 mM glucose for 1 h, and where indicated, the samples were incubated for 30 min, then exposed to UV light for 5 min, and left in the dark for the remainder of 1 h. Data are mean fluorescence/min ± S.E., $n = 3$, all groups. *AU*, arbitrary units.

membranous localization was also seen with NOS-2, and co-localization with capon is highlighted in the merged images (Fig. 10, *lower panels*).

Fluorescence intensity appeared greater for NOS-2 and capon in cells incubated with 20 *versus* 5.5 mM glucose. Therefore, images were quantitatively analyzed after correction for background staining. Capon staining was 30 ± 1.3 ($n = 20$) fluorescence units in cells incubated with 5.5 mM glucose *versus* 42.9 ± 1.2 ($n = 20$, $p < 0.001$) after incubation in 20 mM glucose. Intensity for NOS-2 was 37.9 ± 1.3 in 5.5 mM glucose and 46.9 ± 1.3 ($p < 0.001$) in 20 mM glucose. These differences appear due to alterations in detectable epitopes *versus* more protein, however, because cell content did not differ based on Western blotting normalized to actin content. Capon and NOS-2 in 20 mM glucose-incubated cells were, respectively, 100.1 ± 0.5 ($n = 3$)% and 100.2 ± 1.6 ($n = 3$)% that found in cells incubated with 5.5 mM glucose.

We found that capon influenced the rate of FBE formation. In cell incubated with control siRNA and then exposed to 5.5 mM glucose, the FBE formation rate was 0.8 ± 0.2 (S.E., $n = 3$) fluorescence units/min, and after incubation in 20 mM glucose, 2.5 ± 0.2 (units/min, $n = 3$, $p < 0.05$). In contrast, after depletion of capon using siRNA, cells incubated with 5.5 mM glucose exhibited a FBE formation rate of 0.8 ± 0.2 units/min ($n = 3$) and no significant increase after incubation in 20 mM glucose, 1.0 ± 0.3 units/min ($n = 3$).

Increased NOS activity due to high glucose

NOS-2 activity assessed as conversion of L-[^{3}H]arginine to citrulline inhibitable with 1400W was increased by hyperglycemia. As shown in Table 2, [^{3}H]citrulline production was statistically significantly increased in cells previously treated with the control siRNA and then incubated with 11 or 20 mM glucose *versus* 5.5 mM glucose. However, there was no increased activity with elevated concentrations of glucose using cells depleted of capon. These results are consistent with prior studies showing that NOS-2 activity increases due to cytoskeletal perturbations related to formation of SNO-actin, where depletion or inhibition of the other proteins listed in Fig. 9 have been shown to impede NOS-2 activation (13–15, 43–45).

Discussion

Hyperglycemia causes human and murine neutrophils to increase production of MPs containing high concentrations of IL-1β. There are overlapping roles for reactive species production by mitochondria, Nox, and NOS-2 that lead to actin *S*-nitrosylation and cytoskeletal modifications, including increased proximity of a variety of proteins to short filamentous actin (sF-actin). This conclusion is based on the finding that inhibition/depletion of an enzyme required for reactive species production from one source impedes reactive species production from the alternative sources. This appears to be a common mechanism for MP generation, as the same relationship occurs in response to elevated concentrations of CO_2 and inert gases (13, 14) and in platelets (15). Depletion studies using siRNA indicate that capon also plays a prominent role in the interactive process.

Fig. 1 is a schematic that depicts events we reason to be involved with MP and IL-1β production. The process is likely to start with mitochondrial production of reactive species such as superoxide ($O_2^{\cdot-}$) and H_2O_2 based on assays performed with MitoSOX Red. Although its selectivity for superoxide and for mitochondrial activity is not absolute (46), support that measurements relate to mitochondria comes from finding no enhanced fluorescence using cells depleted of the mitochondrial protein UCP2 or when incubated with genepin (Table 1). UCPs influence cell respiration by partially dissipating the proton electrochemical gradient across the mitochondrial membrane, which diminishes oxidant generation (47, 48). However, UCP2 is also a component of the mitochondrial Ca^{2+} uniporter and preferentially contributes to mitochondrial Ca^{2+} uptake in response to intracellular Ca^{2+} mobilization from the endoplasmic reticulum (49). This is critical for cytosolic Ca^{2+} modulation, enabling mitochondria to transmit Ca^{2+} for utilization from areas of high to low concentration within the cell (49).

The inhibitor and siRNA depletion studies also indicate roles for endoplasmic reticulum IP_3 receptors, which are sensitized by mitochondrial oxidants (50), and for protein kinase C isoforms that can increase Nox activity (13, 51). We interpret studies showing an increase in DCF fluorescence as requiring Nox activation because the enhanced rate of fluorescence did not occur when cells were depleted of gp91phox by siRNA or when co-incubated with the inhibitor Nox2ds (Table 1).

We include an *arrow* in Fig. 1 showing Nox-derived $H_2O_2/O_2^{\cdot-}$ feedback to cause further mitochondrial oxidant production, as well as reacting with nitric oxide ($^{\cdot}$NO) to produce agents capable of protein *S*-nitrosylation (SNO), leading to formation of cytosolic SNO-actin. These relations are supported by the data in Table 1, and the interactions have been shown in response to other stimuli (13, 14, 16).

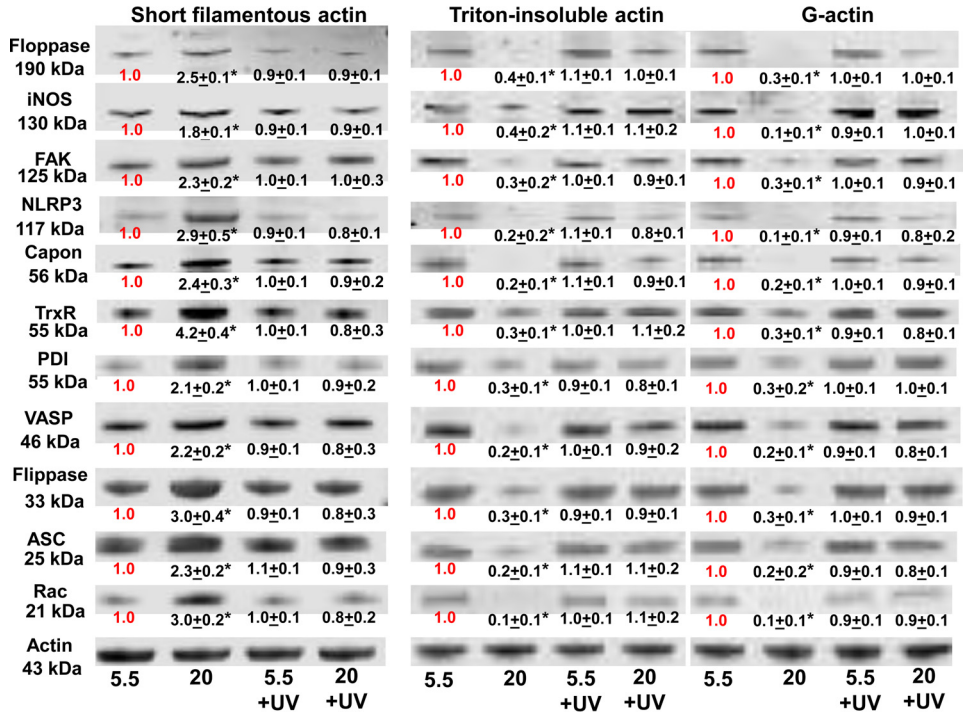

Figure 9. Protein associations in the Triton-soluble short F-actin, G-actin, and Triton-insoluble actin fractions. Murine neutrophils were incubated with buffer containing 5.5 or 20 mM glucose for 1 h, and where indicated, the samples were exposed to UV light between 30 and 35 min of the 1-h incubation, prior to addition of DTSP, to cross-link the proteins. Samples were then fractioned based on Triton solubility (see "Experimental procedures") and subjected to Western blotting. Representative blots among three replicate experiments are shown. After Western blotting, protein band densities were quantified and normalized to the actin band in each lysate. The ratio of each protein relative to actin was compared with that calculated for the 5.5 mM glucose neutrophils in each experiment. Therefore, data in the figure show the fold-change in band density normalized to the ratio observed in 5.5 mM glucose (control) cells for each actin fraction. Data are mean ± S.E. ($n = 3$); *, $p < 0.05$ *versus* cells incubated in 5.5 mM glucose and not exposed to UV light.

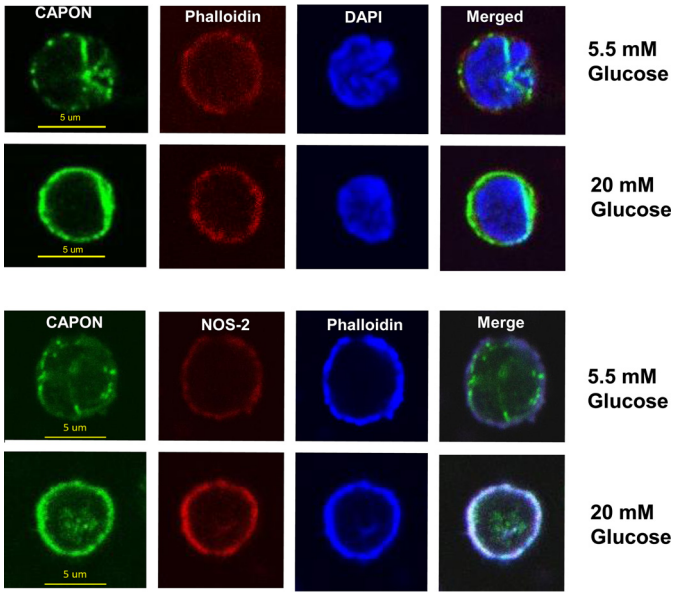

Figure 10. Confocal microscope images of neutrophils. Murine neutrophils were exposed to 5.5 or 20 mM glucose in buffer for 2 h, then fixed, permeabilized, and stained as described under "Experimental procedures." Images are typical from at least three replicate trials using different neutrophil preparations.

Table 2
Nitric-oxide synthase activity

Data are shown in femtomoles of [^{3}H]citrulline production/h by 2.0×10^5 murine neutrophils previously treated with control siRNA or siRNA to deplete capon, and 23 h later incubated with 5.5, 11, or 20 mM glucose. Values are mean ± S.E. ($n = 3$–6 for each data point). *, $p < 0.05$ *versus* 5.5 mM; **, $p < 0.05$ *versus* 5.5 and 11 mM glucose.

	5.5 mM	11 mM	20 mM
Control siRNA	50.7 ± 1.2	98.8 ± 0.1*	138.0 ± 0.8**
Capon siRNA	57.4 ± 1.1	56.4 ± 0.1	56.5 ± 0.1

The second cycle in Fig. 1 pertains to cytoskeletal events. Initial actin polymerization is known to be slow, but it is accelerated in the presence of short actin filaments (52). VASP plays a major role in actin dynamics, as it both bundles filaments and enhances actin polymerization (53). Because VASP exhibits higher affinity for *S*-nitrosylated actin than un-modified actin, we believe this is the stimulus leading to enhanced actin turnover (44). The inhibitory effect of UV light on the entire cascade supports this interpretation. VASP also bundles Rac 1 and 2 with actin and in so doing enhances Rac activation (54, 55). The consequent accelerated actin polymerization hastens linkage of FAK (44, 56, 57). Additionally, FAK has been reported to induce Nox activation (58), and we have previously shown that by linking NOS-2 to sF-actin, FAK increases NOS-2 activity and accelerates MP production formation by neutrophils (14, 44).

The inhibitory effects related to depleting ASC and pro-IL-1β and the use of the caspase inhibitor (see Table 1) are consistent with previous studies (13), and they indicate that components of the NLRP3 inflammasome influence MP generation as well as the various pathways of reactive chemical species generation. Others have reported that caspase 1, which is activated in conjunction with aggregation of inflammasome components, can activate Nox at the phagocytic vacuole membrane in neutrophils and can influence NOS-2 activation, as

well as its synthesis in a complex manner (59, 60). NLRP3 activation in response to oxidative stress is well known (17). Our data indicate there is a two-way communication, wherein activated NLRP3 can also increase reactive chemical species and cell oxidative stress, as we show in Fig. 1.

The intimate linkage between NLRP3/caspase activation and the oxidative stress events is likely to contribute to the potential for pathophysiological consequences to MP production formation in diabetes. Our findings add mechanistic insight to the recognized association of IL-1β to feed-forward amplification of inflammation and exacerbation of type 2 diabetes (24). There are, of course, alternative inflammasomes that activate caspase 1 to impact interleukin and reactive species generation, including NLRP-1b, -3, -4 and AIM2 (absent in melanoma 2) (60). Their potential roles in MP production formation and hyperglycemia will require additional study.

The cross-linking studies (Fig. 9) demonstrate that high glucose increases sF-actin association with an array of proteins known to influence cytoskeletal polymerization, such as VASP, FAK, and Rac. Additional proteins linked to sF-actin include PDI (which is known to facilitate Nox activation (61)), TrxR (which participates in SNO-actin dynamics in a complex manner (44, 56)), and the phospholipid transporters flippase and floppase. MP production formation is recognized to involve cytoskeletal turnover and exposure of phosphatidylserine on the membrane surface due to translocation exerted by activated floppase(s) with inhibition of flippase(s) activity and activation of scramblase by calcium influx (62, 63). High glucose also leads to ASC linkage to sF-actin, similar to other stimuli where subsequent linkage of all inflammasome components to the ASC platform leads to production of active IL-1β (13).

Data demonstrate that capon comes into proximity of sF-actin in response to high glucose, thus placing it close to NOS-2. Clearly, capon influences NOS-2 activation (Table 2) by hyperglycemia, but because of the complex interplay among Nox, mitochondria, and NOS-2, capon influences all of these components. This is consistent with the finding that capon depletion also impedes actin turnover in response to high glucose.

We demonstrate that MP generation and NLRP3 activation in response to hyperglycemia involves *S*-nitrosylation, as both are inhibited with UV exposure. Protein nitration is also triggered by hyperglycemia. Indeed, peroxynitrite has been linked to IL-1β synthesis/secretion by monocytes (64). However, because this modification is not reversed by UV light, we conclude that nitration reactions alone cannot explain MPs and the inflammasome responses to hyperglycemia. With regard to nitration/*S*-nitrosylation targets, there were few protein bands identified in response to hyperglycemia. We have noted similar discrete *S*-nitrosylation of actin in other studies, and we speculate this may be largely due to the co-localization of NOS-2 to filamentous actin (13, 43, 45). Subcellular localization of enzymes generating reactive nitrogen and oxygen species has certainly been shown to influence tyrosine nitration (65). *S*-Nitrosylation can also be influenced by protein acid/base motifs and hydrophobic pockets (66).

The pathways identified may explain how both MP elevations and NLRP3 activation arise in diabetes, supporting the pathophysiological relevance of this study (3–7, 21–23). Importantly, these biochemical responses to hyperglycemia occur within 2 h, which is remarkably fast. Monocytes can begin releasing IL-1β in about 4 h in response to Toll-like receptor agonists and ramp up production over the ensuing 20–40 h (67). NLRP3 inflammasome activation is classically considered a two-step process requiring both transcriptional priming and post-translational activation to generate functional cytokines, and even the alternative non-canonical activation pathway appears to require 14 h (68).

The NLRP3 inflammasome produces active IL-1β and IL-18, but there are distinct differences in processing and secretion of these cytokines (69). Contrary to IL-1β, IL-18 secretion has been shown to occur independent of ROS production in dendritic cells, and IL-18 is found free in plasma (not within lipid vesicles) (67, 70). These differences may explain why we did not find elevations in IL-18 in MPs generated by hyperglycemia.

There are a wide variety of surface proteins on MPs in those with diabetes, suggesting that numerous cell types are activated and contribute to MP elevations (2). Indeed, after a variety of insults, pathological effects have been described due to MPs from platelets (71, 72), monocyte/macrophages (6, 8, 73, 74), and neutrophils (9–11). However, once formed, the MPs appear to interact *in vivo* and to share surface proteins (75). Therefore, when multiple proteins are present, the cell responsible for generating individual MPs cannot be clearly discerned. Additionally, it appears that MPs produced by neutrophils and platelets in response to at least some stimuli are prone to trigger production of MPs from other cell types (76). Whether cells other than neutrophils respond to hyperglycemia and produce MPs is clearly unknown. Thus, the *in vivo* cause–effect relationships for MPs are likely to be blurred.

The clinical relevance of neutrophil-derived MPs to diabetic vasculopathy will require substantial additional study. Capon participates in the complex events leading to production of MPs and IL-1β. This offers a feasible pathophysiological explanation for reports showing that certain capon SNPs are highly associated with impairment of wound healing (25, 26). It is interesting that monocytes do not generate MPs in response to hyperglycemia. We found a similar response to elevated CO_2, and the reasons will require further research (13).

Finally, a recent report using capon-KO *versus* wild-type mice showed enhanced H_2O_2 production in cardiac tissue, and an enhanced occurrence of lethal cardiac dysrhythmias triggered by oxidative stress (77). Effects were thought to arise from perturbation of calcium flux due to capon influence on localization of NOS-1 to cardiac sarcoplasmic reticulum. These data indicate that capon serves an anti-oxidant role in cardiac tissue, whereas our results indicate a pro-oxidative influence in neutrophils. If the general function of capon is to influence NOS activity, then quite different effects based on cell/tissue type as well as NOS isoforms can be expected. We may even speculate that the impaired stem cell mobilization observed with certain capon SNPs may be related to an influence on NOS-3, which plays a major role in mobilization responses (26, 78).

Experimental procedures

Materials

The majority of chemicals and their sources have been listed in prior publications (13, 14). A list of antibodies and manufacturers can be found in supplemental Table 1, and information on small inhibitory RNA (siRNA) is shown in supplemental Table 2.

Studies with human blood

All procedures were reviewed and approved by the University Committee on Studies Involving Human Beings. Subjects were healthy adults who had taken no medications for at least 4 days prior to phlebotomy. Blood was acquired in heparinized tubes.

Animals

All aspects of this study were reviewed and approved by the Institutional Animal Care and Use Committee and with adherence to the Guide for the Care and Use of Laboratory Animals (National Institutes of Health). C57BL/6J mice *(Mus musculus)* were purchased from The Jackson Laboratory (Bar Harbor, ME), housed in the university animal facility, fed a standard rodent diet Laboratory Rodent Diet 5001 (PMI Nutritional Inc., Brentwood, MO), and water *ad libitum*. NOS-2 KO mice (which have a C57BL/6J background) were housed and fed the same as wild-type mice. Mice were anesthetized (intraperitoneal administration of ketamine (100 mg/kg) and xylazine (10 mg/kg)). Skin was prepared by swabbing with Betadine®, and blood was obtained into heparinized syringes by aortic puncture.

Isolation of leukocytes followed by exposure to various agents

Heparin-anticoagulated blood (4 ml) from healthy human volunteers was centrifuged through a two-layer preparation of Histopaque 1077 and 1119 (Sigma) at 400 × *g* for 30 min to isolate monocytes and neutrophils. Murine cells were isolated from heparinized blood of anesthetized mice as described previously (43). At the termination of each experiment, leukocyte viability was determined as trypan blue exclusion using a Countess automated cell counter (Invitrogen).

All studies were done at room temperature. Isolated leukocytes were suspended in PBS buffer, phosphate-buffered saline + 1 mM $CaCl_2$, 1.5 mM $MgCl_2$ containing either 5.5, 11, or 20 mM glucose. Where indicated, prior to studies, some murine cell suspensions were exposed in PBS buffer for 20 h at room temperature to 0.08 nM small inhibitory (siRNA) following the manufacturer's instructions using control siRNA that does not cause specific degradation of any known cellular mRNA or siRNA specific for mouse capon, gp91phox, mitochondrial uncoupling protein 2 (UCP2), type 2 IP_3, or apoptosis-associated Speck protein with CARD domain (ASC). The degree of protein reduction after these treatments was assessed by Western blotting. Where indicated, inhibitors were present in cell suspensions as follows: 5 μM genepin (UCP inhibitor); 1 mM 1400W (NOS-2 inhibitor); 100 μM 2-aminoethoxydiphenyl borate (IP_3 inhibitor); 5 μM GF 109203X (PKC inhibitor); 10 μM Nox2ds (NOX inhibitor); or 10 μM of the scrambled sequence control peptide to Nox2ds. In other experiments during incubations but prior to specific studies, cell suspensions were illuminated at room temperature for 5 min with a mercury vapor UV lamp (Blak-Ray B-100A, Ultraviolet Products, Inc., San Gabriel, CA) following published procedures (13).

Generation of reactive species

After incubation in different glucose concentrations, leukocyte suspensions were prepared with 10 μM 2,7-dihydrodichlorofluorescein-diacetate (DCF-DA), and fluorescence was monitored (492 nm excitation and 530 nm emission) as described previously (14). Because DCF can autocatalyze its own oxidation (79), in all studies DCF-DA was added immediately prior to performing the fluorescence assay.

Actin polymerization and NOS activity assays of permeabilized neutrophils

Neutrophil suspensions were permeabilized using 0.2% *n*-octyl-β-glucopyranoside and then exposed to different glucose concentrations. Actin polymerization assessed using pyrene-actin and NOS activity assessed without or with 0.1 μM 1400W (NOS-2 inhibitor) was carried out exactly as described previously (14).

Cytoskeletal protein associations based on Triton solubility

After exposure to different glucose concentrations, 0.5 mM DTSP was added to neutrophil suspensions to cross-link sulfhydryl-containing proteins within a proximity of ~12 Å following published procedures (43). Cell lysates were partitioned into Triton-soluble G-actin and short F-actin and Triton-insoluble protein fractions and subjected to electrophoresis in gradient 4–15% SDS-polyacrylamide gels followed by Western blotting as described previously (43).

Cell extract preparation and biotin-switch assay

After different glucose concentrations, neutrophil suspensions were transferred to HEN buffer (250 mM Hepes, pH 7.7, 1 mM EDTA, 0.1 mM neocuproine), lysed, and subjected to the biotin-switch assay as described previously (43).

Flow cytometry

MPs were analyzed as described in previous publications (75, 80). In brief, flow cytometry was performed with an 8-color, triple laser MACSQuant® analyzer (Miltenyi Biotec Corp., Auburn, CA) using MACSQuantify™ software version 2.5 to analyze data. MACSQuant was calibrated every other day with calibration beads ((Miltenyi Biotec Corp., Auburn, CA). Forward and side scatter were set at logarithmic gain. Photomultiplier tube voltage and triggers were optimized to detect submicron particles. Micro-beads of three different diameters, 0.3 (Sigma), 1.0, and 3.0 μm (Spherotech, Inc., Lake Forest, IL), were used for initial settings and before each experiment as an internal control. Samples were suspended in annexin binding buffer solution (1:10 v/v in distilled water) (Pharmingen), and antibodies as listed in supplemental Table 2, with positive staining determined following the fluorescence-minus-one control test. All reagents and solutions used for MP analysis were sterile and filtered (0.1 μm filter). MPs were defined as annexin V-pos-

itive particles with diameters of 0.3–1-μm diameter. In this way, smaller particles that may include exosomes ($<$0.1 μm diameter, an alternative way IL-1β can be packaged for exocytosis (81)) and non-vesicle protein aggregates were excluded. The concentration of MPs in sample tubes was determined by MACSQuant® analyzer according to exact volume of solution from which MPs were analyzed.

IL-1β and IL-18 measurements

Human and mouse-specific IL-1β (eBioscience, San Diego) and mouse-specific IL-18 (eBioscience, San Diego) ELISA kits were used to evaluate cytokines in MP samples following the manufacturer's instructions. MPs were first prepared the same as for flow cytometry analysis but were then centrifuged at 100,000 $\times g$ for 60 min, and the MP pellets were lysed with 0.3 ml of lysis buffer (20 mM Tris, 150 mM NaCl, 1% Nonidet P-40, 0.5% sodium deoxycholate, 1 mM EDTA, and 0.1% SDS, pH 7.5, with protease inhibitors mixture (Sigma)). The protein content of the sample was measured and diluted to 5 mg/ml, and 20 μg of protein was used in the assays.

Mass spectrometry

Protein identification by mass spectrometry (MS) was performed at the Mass Spectrometry Center, University of Maryland School of Pharmacy. Protein bands identified as containing biotin or nitrotyrosine on Western blottings were excised from an SDS-polyacrylamide gel, alkylated, and digested by trypsin and LysC. Tryptic peptides were separated on a Waters nanoACQUITY UPLC system with an ACQUITY UPLC M-class CSH C_{18} column and analyzed on a coupled Orbitrap Fusion Tribrid mass spectrometer (Thermo Fisher Scientific) as described by Williamson *et al.* (82). Tandem mass spectra were searched against UniProt mouse reference proteome (*M. musculus* C57BL/6J, UP000000589) using a SEQUEST HT algorithm described by Eng *et al.* (83). Resulting hits were validated at a maximum false discovery rate of 0.01 using a semi-supervised machine learning algorithm Percolator developed by Käll *et al.* (84).

Confocal microscopy

Isolated neutrophils were placed on fibrinogen-coated glass slides and incubated at 37 °C for 1 h; followed by fixation with 4% paraformaldehyde at room temperature for 30 min. Cells were rinsed three times with PBS and then permeabilized and blocked by incubation for 1 h at room temperature with PBS containing 0.2% (v/v) Triton X-100, 0.3% (v/v) glycine, 5% (v/v) normal goat serum, and 5% (v/v) fetal bovine serum. Cells were then incubated with a 1:50 dilution of anti-capon rabbit monoclonal IgG antibody and anti-NOS-2 mouse monoclonal IgG plus 1:200 Alexa 647-conjugated phalloidin in room temperature for 2 h. After rinsing three times with PBS, the slides were incubated with a 1:200 dilutions of Alexa 488-conjugated goat anti-rabbit IgG and Alexa 647-conjugated goat anti-mouse Ig for 1 h followed in some studies by counterstaining with 4′,6-diamidino-2-phenylindole (DAPI).

Images of neutrophils were acquired using a Nikon inverted stage confocal microscope equipped with a Plan-Apochromat 63/1.4 numerical aperture oil objective. Fluorophore excitation was provided by 405-, 488- and 633-nm laser lines, and resulting fluorescence was separated using 420–480-, 505-, and 650-nm bandpass filters.

Statistical analysis

Results are expressed as the mean ± S.E. for three or more independent experiments. Data were compared by analysis of variance using SigmaStat (Jandel Scientific, San Jose, CA) and Newman-Keuls post hoc test. The level of statistical significance was defined as $p < 0.05$.

Author contributions—V. M. B., K. Y., W. H., and M. A. K. performed laboratory studies, interpreted data, reviewed the manuscript, provided advice, and approved the final version of the manuscript. D. J. M. conceived ideas, reviewed the manuscript, provided advice, and approved the final version of the manuscript. S. R. T. conceived ideas and oversaw the research program, performed laboratory studies, analyzed data, interpreted data, and wrote the manuscript.

References

1. Enjeti, A. K., Lincz, L. F., and Seldon, M. (2007) Detection and measurement of microparticles: an evolving research tool for vascular biology. *Semin. Thromb. Hemost.* **33,** 771–779
2. Li, S., Wei, J., Zhang, C., Li, X., Meng, W., Mo, X., Zhang, Q., Liu, Q., Ren, K., Du, R., Tian, H., and Li, J. (2016) Cell-derived microparticles in patients with type 2 diabetes mellitus: a systematic review and meta-analysis. *Cell Physiol. Biochem.* **39,** 2439–2450
3. Alexandru, N., Badila, E., Weiss, E., Cochior, D., Stepień, E., and Georgescu, A. (2016) Vascular complications in diabetes: microparticles and microparticle associated microRNAs as active players. *Biochem. Biophys. Res. Commun.* **472,** 1–10
4. Koga, H., Sugiyama, S., Kugiyama, K., Watanabe, K., Fukushima, H., Tanaka, T., Sakamoto, T., Yoshimura, M., Jinnouchi, H., and Ogawa, H. (2005) Elevated levels of VE-cadherin-positive endothelial microparticles in patients with type 2 diabetes mellitus and coronary artery disease. *J. Am. Coll. Cardiol.* **45,** 1622–1630
5. Tan, K. T., Tayebjee, M. H., Lim, H. S., and Lip, G. Y. (2005) Clinically apparent atherosclerotic disease in diabetes is associated with an increase in platelet microparticle levels. *Diabet. Med.* **22,** 1657–1662
6. Ogata, N., Nomura, S., Shouzu, A., Imaizumi, M., Arichi, M., and Matsumura, M. (2006) Elevation of monocyte-derived microparticles in patients with diabetic retinopathy. *Diabetes Res. Clin. Pract.* **73,** 241–248
7. Diamant, M., Nieuwland, R., Pablo, R. F., Sturk, A., Smit, J. W., and Radder, J. K. (2002) Elevated numbers of tissue-factor exposing microparticles correlate with components of the metabolic syndrome in uncomplicated type 2 diabetes mellitus. *Circulation* **106,** 2442–2447
8. Niu, C., Wang, X., Zhao, M., Cai, T., Liu, P., Li, J., Willard, B., Zu, L., Zhou, E., Li, Y., Pan, B., Yang, F., and Zheng, L. (2016) Macrophage foam cell-derived extracellular vesicles promote vascular smooth muscle cell migration and adhesion. *J. Am. Heart Assoc.* **5,** e004099
9. Slater, T. W., Finkielsztein, A., Mascarenhas, L. A., Mehl, L. C., Butin-Israeli, V., and Sumagin, R. (2017) Neutrophil microparticles deliver active myeloperoxidase to injured mucosa to inhibit epithelial wound healing. *J. Immunol.* **198,** 2886–2897
10. Pitanga, T. N., de Aragão França, L., Rocha, V. C., Meirelles, T., Borges, V. M., Gonçalves, M. S., Pontes-de-Carvalho, L. C., Noronha-Dutra, A. A., and dos-Santos, W. L. (2014) Neutrophil-derived microparticles induce myeloperoxidase-mediated damage of vascular endothelial cells. *BMC Cell Biol.* **15,** 21
11. Butin-Israeli, V., Houser, M. C., Feng, M., Thorp, E. B., Nusrat, A., Parkos, C. A., and Sumagin, R. (2016) Deposition of microparticles by neutrophils onto inflamed epithelium: a new mechanism to disrupt epithelial intercel-

lular adhesions and promote transepithelial migration. *FASEB J.* **30,** 4007–4020
12. Brownlee, M. (2005) The pathophysiology of diabetic complications: a unifying mechanism. *Diabetes* **54,** 1615–1625
13. Thom, S. R., Bhopale, V. M., Hu, J., and Yang, M. (2017) Increased carbon dioxide levels stimulate neutrophils to produce microparticles and activate the nucleotide-binding domain-like receptor 3 inflammasome. *Free Radic. Biol. Med.* **106,** 406–416
14. Thom, S. R., Bhopale, V. M., and Yang, M. (2014) Neutrophils generate microparticles during exposure to inert gases due to cytoskeletal oxidative stress. *J. Biol. Chem.* **289,** 18831–18845
15. Bhullar, J., Bhopale, V. M., Yang, M., Sethuraman, K., and Thom, S. R. (2016) Microparticle formation by platelets exposed to high gas pressures–an oxidative stress response. *Free Radic. Biol. Med.* **101,** 154–162
16. Dikalov, S. (2011) Cross talk between mitochondria and NADPH oxidases. *Free Radic. Biol. Med.* **51,** 1289–1301
17. Abderrazak, A., Syrovets, T., Couchie, D., El Hadri, K., Friguet, B., Simmet, T., and Rouis, M. (2015) NLRP3 inflammasome: from a danger signal sensor to a regulatory node of oxidative stress and inflammatory diseases. *Redox Biol.* **4,** 296–307
18. MacKenzie, A., Wilson, H. L., Kiss-Toth, E., Dower, S. K., North, R. A., and Surprenant, A. (2001) Rapid secretion of interleukin-1 by microvesicle shedding. *Immunity* **15,** 825–835
19. Bianco, F., Pravettoni, E., Colombo, A., Schenk, U., Möller, T., Matteoli, M., and Verderio, C. (2005) Astrocyte-derived ATP induces vesicle shedding and IL-1 release from microglia. *J. Immunol.* **174,** 7268–7277
20. Pizzirani, C., Ferrari, D., Chiozzi, P., Adinolfi, E., Sandonà, D., Savaglio, E., and Di Virgilio, F. (2007) Stimulation of P2 receptors causes release of IL-1-loaded microvesicles from human dendritic cells. *Blood* **109,** 3856–3864
21. Chen, W., Zhao, M., Zhao, S., Lu, Q., Ni, L., Zou, C., Lu, L., Xu, X., Guan, H., Zheng, Z., and Qiu, Q. (2017) Activation of the TXNIP/NLRP3 inflammasome pathway contributes to inflammation in diabetic retinopathy: a novel inhibitory effect of minocycline. *Inflamm. Res.* **66,** 157–166
22. Chen, Y., Wang, L., Pitzer, A. L., Li, X., Li, P. L., and Zhang, Y. (2016) Contribution of redox-dependent activation of endothelial Nlrp3 inflammasomes to hyperglycemia-induced endothelial dysfunction. *J. Mol. Med.* **94,** 1335–1347
23. Qiu, Y. Y., and Tang, L. Q. (2016) Roles of the NLRP3 inflammasome in the pathogenesis of diabetic nephropathy. *Pharmacol. Res.* **114,** 251–264
24. Sauter, N. S., Schulthess, F. T., Galasso, R., Castellani, L. W., and Maedler, K. (2008) The antiinflammatory cytokine interleukin-1 receptor antagonist protects from high-fat diet-induced hyperglycemia. *Endocrinology* **149,** 2208–2218
25. Margolis, D. J., Gupta, J., Thom, S. R., Townsend, R. R., Kanetsky, P. A., Hoffstad, O., Papdopoulos, M., Fischer, M., Schelling, J. R., and Mitra, N. (2013) Diabetes, lower extremity amputation, loss of protective sensation, and neuronal nitric oxide associated protein in the chronic renal insufficiency cohort study. *Wound Repair Regen.* **21,** 17–24
26. Margolis, D. J., Hampton, M., Hoffstad, O., Malay, D. S., Mirza, Z., Woltereck, D., Shannon, S., Troiano, M., Mitra, N., Yang, M., Bhopale, V. M., and Thom, S. R. (2017) NOS1AP genetic variation is associated with impaired healing of diabetic foot ulcers and diminished response to healing of circulating stem/progenitor cells. *Wound Repair Regen.* 10.1111/wrr.12564
27. Becker, M. L., Aarnoudse, A. J., Newton-Cheh, C., Hofman, A., Witteman, J. C., Uitterlinden, A. G., Visser, L. E., and Stricker, B. H. (2008) Common variation in the NOS1AP gene is associated with reduced glucose-lowering effect and with increased mortality in users of sulfonylurea. *Pharmacogenet. Genomics* **18,** 591–597
28. Chu, A. Y., Coresh, J., Arking, D. E., Pankow, J. S., Tomaselli, G. F., Chakravarti, A., Post, W. S., Spooner, P. H., Boerwinkle, E., and Kao, W. H. (2010) NOS1AP variant associated with incidence of type 2 diabetes in calcium channel blocker users in the Atherosclerosis Risk in Communities (ARIC) study. *Diabetologia* **53,** 510–516
29. Qin, W., Zhang, R., Hu, C., Wang, C. R., Lu, J. Y., Yu, W. H., Bao, Y. Q., Xiang, K. S., International Type 2 Diabetes 1q Consortium, and Jia, W. P. (2010) A variation in NOS1AP gene is associated with repaglinide efficacy on insulin resistance in type 2 diabetes of Chinese. *Acta Pharmacol. Sin.* **31,** 450–454
30. Wang, T., Wang, Y., Lv, D. M., Song, J. F., Lu, Q., Gao, X., Zhang, F., Guo, H., Li, W., and Yin, X. X. (2014) Effects of NOS1AP rs12742393 polymorphism on repaglinide response in Chinese patients with type 2 diabetes mellitus. *Pharmacotherapy* **34,** 131–139
31. Andreasen, C. H., Mogensen, M. S., Borch-Johnsen, K., Sandbaek, A., Lauritzen, T., Almind, K., Hansen, L., Jørgensen, T., Pedersen, O., and Hansen, T. (2008) Lack of association between PKLR rs3020781 and NOS1AP rs7538490 and type 2 diabetes, overweight, obesity and related metabolic phenotypes in a Danish large-scale study: case-control studies and analyses of quantitative traits. *BMC Med. Genet.* **9,** 118
32. Hu, C., Wang, C., Zhang, R., Ng, M. C., Bao, Y., Wang, C., So, W. Y., Ma, R. C., Ma, X., Chan, J. C., Xiang, K., and Jia, W. (2010) Association of genetic variants of NOS1AP with type 2 diabetes in a Chinese population. *Diabetologia* **53,** 290–298
33. Zhang, Y., Endam, L. M., Filali-Mouhim, A., Bossé, Y., Castano, R., and Desrosiers, M. (2011) Polymorphisms in the nitric-oxide synthase 1 gene are associated with severe chronic rhinosinusitis. *Am. J. Rhinol. Allergy* **25,** e49–e54
34. Armstrong, D. G., Kanda, V. A., Lavery, L. A., Marston, W., Mills, J. L., Sr., and Boulton, A. J. (2013) Mind the gap: disparity between research funding and costs of care for diabetic foot ulcers. *Diabetes Care* **36,** 1815–1817
35. Courtney, M. J., Li, L. L., and Lai, Y. Y. (2014) Mechanisms of NOS1AP action on NMDA receptor-nNOS signaling. *Front. Cell Neurosci.* **8,** 252
36. Jaffrey, S. R., Snowman, A. M., Eliasson, M. J., Cohen, N. A., and Snyder, S. H. (1998) CAPON: a protein associated with neuronal nitric-oxide synthase that regulates its interactions with PSD95. *Neuron* **20,** 115–124
37. Carrel, D., Hernandez, K., Kwon, M., Mau, C., Trivedi, M. P., Brzustowicz, L. M., and Firestein, B. L. (2015) Nitric-oxide synthase 1 adaptor protein, a protein implicated in schizophrenia, controls radial migration of cortical neurons. *Biol. Psychiatry* **77,** 969–978
38. Wang, J., Jin, L., Zhu, Y., Zhou, X., Yu, R., and Gao, S. (2016) Research progress in NOS1AP in neurological and psychiatric diseases. *Brain Res. Bull.* **125,** 99–105
39. Clattenburg, L., Wigerius, M., Qi, J., Rainey, J. K., Rourke, J. L., Muruganandan, S., Sinal, C. J., and Fawcett, J. P. (2015) NOS1AP functionally associates with YAP To regulate Hippo signaling. *Mol. Cell. Biol.* **35,** 2265–2277
40. Chen, M., Cheng, C., Yan, M., Niu, S., Gao, S., Shi, S., Liu, H., Qin, Y., and Shen, A. (2008) Involvement of capon and nitric-oxide synthases in rat muscle regeneration after peripheral nerve injury. *J. Mol. Neurosci.* **34,** 89–100
41. Martinon, F., Burns, K., and Tschopp, J. (2002) The inflammasome: a molecular platform triggering activation of inflammatory caspases and processing of proIL-β. *Mol. Cell* **10,** 417–426
42. Lu, A., Magupalli, V. G., Ruan, J., Yin, Q., Atianand, M. K., Vos, M. R., Schröder, G. F., Fitzgerald, K. A., Wu, H., and Egelman, E. H. (2014) Unified polymerization mechanism for the assembly of ASC-dependent inflammasomes. *Cell* **156,** 1193–1206
43. Thom, S. R., Bhopale, V. M., Mancini, D. J., and Milovanova, T. N. (2008) Actin *S*-nitrosylation inhibits neutrophil β2 integrin function. *J. Biol. Chem.* **283,** 10822–10834
44. Thom, S. R., Bhopale, V. M., Milovanova, T. N., Yang, M., Bogush, M., and Buerk, D. G. (2013) Nitric-oxide synthase-2 linkage to focal adhesion kinase in neutrophils influences enzyme activity and β-2 integrin function. *J. Biol. Chem.* **288,** 4810–4818
45. Bhopale, V. M., Yang, M., Yu, K., and Thom, S. R. (2015) Factors associated with nitric oxide-mediated β-2 integrin inhibition of neutrophils. *J. Biol. Chem.* **290,** 17474–17484
46. Zielonka, J., and Kalyanaraman, B. (2010) Hydroethidine- and MitoSOX-derived red fluorescence is not a reliable indicator of intracellular super-

oxide formation: another inconvenient truth. *Free Radic. Biol. Med.* **48,** 983–1001
47. Qiao, C., Wei, L., Dai, Q., Zhou, Y., Yin, Q., Li, Z., Xiao, Y., Guo, Q., and Lu, N. (2015) UCP2-related mitochondrial pathway participates in oroxylin A-induced apoptosis in human colon cancer cells. *J. Cell Physiol.* **230,** 1054–1063
48. Giardina, T. M., Steer, J. H., Lo, S. Z., and Joyce, D. A. (2008) Uncoupling protein-2 accumulates rapidly in the inner mitochondrial membrane during mitochondrial reactive oxygen stress in macrophages. *Biochim. Biophys. Acta* **1777,** 118–129
49. Waldeck-Weiermair, M., Malli, R., Naghdi, S., Trenker, M., Kahn, M. J., and Graier, W. F. (2010) The contribution of UCP2 and UCP3 to mitochondrial Ca^{2+} uptake is differentially determined by the source of supplied Ca^{2+}. *Cell Calcium* **47,** 433–440
50. Bánsághi, S., Golenár, T., Madesh, M., Csordás, G., RamachandraRao, S., Sharma, K., Yule, D. I., Joseph, S. K., and Hajnóczky, G. (2014) Isoform- and species-specific control of inositol 1,4,5-triphosphate (IP_3) receptors by reactive oxygen species. *J. Biol. Chem.* **289,** 8170–8181
51. El Jamali, A., Valente, A. J., and Clark, R. A. (2010) Regulation of phagocyte NADPH oxidase by hydrogen peroxide through a Ca^{2+}/c-Abl signaling pathway. *Free Radic. Biol. Med.* **48,** 798–810
52. Lal, A. A., Korn, E. D., and Brenner, S. L. (1984) Rate constants for actin polymerization in ATP determined using cross-linked actin trimers as nuclei. *J. Biol. Chem.* **259,** 8794–8800
53. Bearer, E. L., Prakash, J. M., Manchester, R. D., and Allen, P. G. (2000) VASP protects actin filaments from gelsolin: an *in vitro* study with implications for platelet actin reorganizations. *Cell Motil. Cytoskeleton* **47,** 351–364
54. Schlegel, N., and Waschke, J. (2009) VASP is involved in cAMP-mediated Rac 1 activation in microvascular endothelial cells. *Am. J. Physiol. Cell Physiol.* **296,** C453–C462
55. Schlegel, N., and Waschke, J. (2009) Impaired integrin-mediated adhesion contributes to reduced barrier properties in VASP-deficient microvascular endothelium. *J. Cell Physiol.* **220,** 357–366
56. Thom, S. R., Bhopale, V. M., Milovanova, T. N., Yang, M., and Bogush, M. (2012) Thioredoxin reductase linked to cytoskeleton by focal adhesion kinase reverses actin *S*-nitrosylation and restores neutrophil β-2 integrin function. *J. Biol. Chem.* **287,** 30346–30357
57. Thom, S. R., Bhopale, V. M., Yang, M., Bogush, M., Huang, S., and Milovanova, T. (2011) Neutrophil β-2 integrin inhibition by enhanced interactions of vasodilator stimulated phosphoprotein with S-nitrosylated actin. *J. Biol. Chem.* **286,** 32854–32865
58. Kasorn, A., Alcaide, P., Jia, Y., Subramanian, K. K., Sarraj, B., Li, Y., Loison, F., Hattori, H., Silberstein, L. E., Luscinskas, W. F., and Luo, H. R. (2009) Focal adhesion kinase regulated pathogen-killing capability and life span of neutrophils via mediating both adhesion-dependent and -independent cellular signals. *J. Immunol.* **183,** 1032–1043
59. Sokolovska, A., Becker, C. E., Ip, W. K., Rathinam, V. A., Brudner, M., Paquette, N., Tanne, A., Vanaja, S. K., Moore, K. J., Fitzgerald, K. A., Lacy-Hulbert, A., and Stuart, L. M. (2013) Activation of caspase-1 by the NLRP3 inflammasome regulates the NADPH oxidase NOX2 to control phagosome function. *Nat. Immunol.* **14,** 543–553
60. Buzzo, C. L., Medina, T., Branco, L. M., Lage, S. L., Ferreira, L. C., Amarante-Mendes, G. P., Hottiger, M. O., De Carvalho, D. D., and Bortoluci, K. R. (2017) Epigenetic regulation of nitric-oxide synthase 2, inducible (Nos2) by NLRC4 inflammasomes involves PARP1 cleavage. *Sci. Rep.* **7,** 41686
61. de A Paes, A. M., Veríssimo-Filho, S., Guimarães, L. L., Silva, A. C., Takiuti, J. T., Santos, C. X., Janiszewski, M., Laurindo, F. R., and Lopes, L. R. (2011) Protein-disulfide isomerase redox-dependent association with p47phox: evidence for an organizer role in leukocyte NADPH oxidase activation. *J. Leukocyte Biol.* **90,** 799–810
62. Wehman, A. M., Poggioli, C., Schweinsberg, P., Grant, B. D., and Nance, J. (2011) The P4-ATPase TAT-5 inhibits the budding of extracellular vesicles in *C. elegans* embryos. *Curr. Biol.* **21,** 1951–1959
63. Bevers, E. M., Comfurius, P., Dekkers, D. W., and Zwaal, R. F. (1999) Lipid translocation across the plasma membrane of mammalian cells. *Biochim. Biophys. Acta* **1439,** 317–330
64. Hewinson, J., Moore, S. F., Glover, C., Watts, A. G., and MacKenzie, A. B. (2008) A key role for redox signaling in rapid P2X7 receptor-induced IL-1β processing in human monocytes. *J. Immunol.* **180,** 8410–8420
65. Heijnen, H. F., van Donselaar, E., Slot, J. W., Fries, D. M., Blachard-Fillion, B., Hodara, R., Lightfoot, R., Polydoro, M., Spielberg, D., Thomson, L., Regan, E. A., Crapo, J., and Ischiropoulos, H. (2006) Subcellular localization of tyrosine-nitrated proteins is dictated by reactive oxygen species generating enzymes and by proximity to nitric-oxide synthase. *Free Radic. Biol. Med.* **40,** 1903–1913
66. Greco, T. M., Hodara, R., Parastatidis, I., Heijnen, H. F., Dennehy, M. K., Liebler, D. C., and Ischiropoulos, H. (2006) Identification of *S*-nitrosylation motifs by site-specific mapping of the *S*-nitrosocysteine proteome in human vascular smooth muscle cells. *Proc. Natl. Acad. Sci. U.S.A.* **103,** 7420–7425
67. Joosten, L. A., Netea, M. G., and Dinarello, C. A. (2013) Interleukin-1β in innate inflammation, autophagy and immunity. *Semin. Immunol.* **25,** 416–424
68. Elliott, E. I., and Sutterwala, F. S. (2016) Monocytes take their own path to IL-1β. *Immunity* **44,** 713–715
69. Puren, A. J., Fantuzzi, G., and Dinarello, C. A. (1999) Gene expression, synthesis, and secretion of interleukin 18 and interleukin 1β are differentially regulated in human blood mononuclear cells and mouse spleen cells. *Proc. Natl. Acad. Sci. U.S.A.* **96,** 2256–2261
70. Schmidt, R. L., and Lenz, L. L. (2012) Distinct licensing of IL-18 and IL-1β secretion in response to NLRP3 inflammasome activation. *PLoS ONE* **7,** e45186
71. Campello, E., Radu, C. M., Duner, E., Lombardi, A. M., Spiezia, L., Bendo, R., Ferrari, S., Simioni, P., and Fabris, F. (2017) Activated platelet-derived and leukocyte-derived circulating microparticles and the risk of thrombosis in heparin-induced thrombocytopenia: a role for PF4-bearing microparticles? *Cytometry B. Clin. Cytom.* 10.1002/cyto.b.21507
72. Bei, J. J., Liu, C., Peng, S., Liu, C. H., Zhao, W. B., Qu, X. L., Chen, Q., Zhou, Z., Yu, Z. P., Peter, K., and Hu, H. Y. (2016) Staphylococcal SSL5-induced platelet microparticles provoke proinflammatory responses via the CD40/TRAF6/NFB signalling pathway in monocytes. *Thromb. Haemost.* **115,** 632–645
73. Chiva-Blanch, G., Bratseth, V., Ritschel, V., Andersen, G. Ø., Halvorsen, S., Eritsland, J., Arnesen, H., Badimon, L., and Seljeflot, I. (2017) Monocyte-derived circulating microparticles (CD14+, CD14+/CD11b+ and CD14+/CD142+) are related to long-term prognosis for cardiovascular mortality in STEMI patients. *Int. J. Cardiol.* **227,** 876–881
74. Wang, J. G., Williams, J. C., Davis, B. K., Jacobson, K., Doerschuk, C. M., Ting, J. P., and Mackman, N. (2011) Monocytic microparticles activate endothelial cells in an IL-1β-dependent manner. *Blood* **118,** 2366–2374
75. Thom, S. R., Yang, M., Bhopale, V. M., Huang, S., and Milovanova, T. N. (2011) Microparticles initiate decompression-induced neutrophil activation and subsequent vascular injuries. *J. Appl. Physiol.* **110,** 340–351
76. Thom, S. R., Milovanova, T. N., Bogush, M., Bhopale, V. M., Yang, M., Bushmann, K., Pollock, N. W., Ljubkovic, M., Denoble, P., and Dujic, Z. (2012) Microparticle production, neutrophil activation and intravascular bubbles following open-water SCUBA diving. *J. Appl. Physiol.* **112,** 1268–1278
77. Sugiyama, K., Sasano, T., Kurokawa, J., Takahashi, K., Okamura, T., Kato, N., Isobe, M., and Furukawa, T. (2016) Oxidative stress induced ventricular arrhythmia and impairment of cardiac function in Nos1ap deleted mice. *Int. Heart J.* **57,** 341–349
78. Aicher, A., Heeschen, C., Mildner-Rihm, C., Urbich, C., Ihling, C., Technau-Ihling, K., Zeiher, A. M., and Dimmeler, S. (2003) Essential role of endothelial nitric-oxide synthase for mobilization of stem and progenitor cells. *Nat. Med.* **9,** 1370–1376
79. Bonini, M. G., Rota, C., Tomasi, A., and Mason, R. P. (2006) The oxidation of 2′,7′-dichlorofluorescein to reactive oxygen species: A self-fulfilling prophesy? *Free Radic. Biol. Med.* **40,** 968–975
80. Yang, M., Milovanova, T. N., Bogush, M., Uzun, G., Bhopale, V. M., and Thom, S. R. (2012) Microparticle enlargement and altered surface pro-

teins after air decompression are associated with inflammatory vascular injuries. *J. Appl. Physiol.* **112,** 204–211
81. Deretic, V., Jiang, S., and Dupont, N. (2012) Autophagy intersections with conventional and unconventional secretion in tissue development, remodeling and inflammation. *Trends Cell Biol.* **22,** 397–406
82. Williamson, J. C., Edwards, A. V., Verano-Braga, T., Schwämmle, V., Kjeldsen, F., Jensen, O. N., and Larsen, M. R. (2016) High-performance hybrid Orbitrap mass spectrometers for quantitative proteome analysis: observations and implications. *Proteomics* **16,** 907–914
83. Eng, J. K., Fischer, B., Grossmann, J., and Maccoss, M. J. (2008) A fast SEQUEST cross correlation algorithm. *J. Proteome. Res.* **7,** 4598–4602
84. Käll, L., Canterbury, J. D., Weston, J., Noble, W. S., and MacCoss, M. J. (2007) Semi-supervised learning for peptide identification from shotgun proteomics datasets. *Nat. Methods* **4,** 923–925